Korean J. Chem. Eng., 34(7), 1905-1913 (2017)
DOI: 10.1007/s11814-017-0025-1

pISSN: 0256-1115
eISSN: 1975-7220

Performance evaluation of a novel reactor configuration for oxidative dehydrogenation of ethane to ethylene

Hamid Asadi-Saghandi* and Javad Karimi-Sabet,†**

*Department of Chemical Engineering, University of Tehran, Tehran, Iran
**NFCRS, Nuclear Science and Technology Research Institute, Tehran, Iran
(*Received 10 November 2016 • accepted 6 February 2017*)

Abstract−A one-dimensional non-isothermal steady state model was developed to simulate the performance of three-reactor configurations for the oxidative dehydrogenation of ethane (ODHE) to ethylene. These configurations consist of side feeding reactor (SFR), conventional fixed bed reactor (CFBR) and membrane reactor (MR). The performance of these reactors was compared in the terms of C_2H_6 conversion, C_2H_4 and CO_2 selectivity and temperature profiles. The use of sectional air injections on the wall of SFR with a limited number of injection points showed that the performance of reactor significantly improves and optimum pattern of oxygen consumption is also obtained. Moreover, our SFR with a liquid coolant medium operates in an effectively controlled temperature profile that is comparable with that of the MR, which is cooled by a coolant stream of air. Hence, an enhancement in the level of selectivity is obtained for the SFR configuration. Consequently, the side feeding procedure can decrease the high operating temperature problem and low ethylene selectivity in the ODHE process. According to obtained results, the SFR would be a proper alternative for both the MR and CFBR.

Keywords: Oxidative Dehydrogenation of Ethane, Side Feeding Reactor, Fixed Bed Reactor, Membrane Reactor, Mathematical Modeling

INTRODUCTION

Ethylene is widely used as a feedstock in the petrochemical industry to produce highly demanded commodities such as polyethylene, ethylene oxide, acetaldehyde, ethanol, and ethylene dichloride. Thermal or catalytic cracking of hydrocarbons is main route to produce ethylene at industrial scale. However, the cracking process is highly endothermic and equilibrium-limited. Furthermore, the rapid coke formation in this process makes it mandatory for the plant to be shut down periodically. The oxidative dehydrogenation of ethane (ODHE) to ethylene as a promising alternative process to produce ethylene has been widely studied [1-6]. The ODHE reactions are irreversible and significantly exothermic reducing energy costs. Moreover, because of the limited number of products, the separation cost of the reaction products decreases considerably [5,7-9].

However, such exothermic reactions release a high amount of energy that can damage catalysts and reactor, leading to runaway reactions. Moreover, the side oxidation reactions, i.e., the ethane combustion and the ethylene combustion, produce a large amount of carbon dioxide which limits the yield of ethylene in the ODHE process. Therefore, it is required to control the operating temperature of the reactor for achieving a desired yield of ethylene and a safe operation in the plant [10-12]. To perform such exothermic processes, multi-tubular fixed bed reactors have been introduced to increase the heat transfer area and decrease the radial gradients by small diameter tubes immersing in a coolant [13]. Researchers have proposed an attractive method which decreases the generated heat and enhances the selectivity and yield of ethylene by maintaining the oxygen concentration in lower levels in the reaction side. For this aim, the oxygen has to be distributed axially along the reactor [7,14].

Membrane reactors are being widely used by many researchers due to their ability to perform simultaneously reaction and separation in one apparatus [15,16]. Furthermore, in membrane reactors, oxygen can be uniformly injected through the reactor creating an efficient concentration profile of oxygen along the reaction side, reducing the operating temperature and enhancing the yield of desired products. However, membrane reactors have some drawbacks such as low conversion of the reactants and provoking flammable mixtures in some operating conditions due to the accumulation of O_2. Moreover, membrane fouling could alter the properties of membrane with the passage of time. There are also some problems such as mechanical strength problem and high construction cost that limit the industrial applications of this type of reactors [7, 17-21].

Nevertheless, fixed bed reactors are commonly employed in chemical industries because of their low operating costs and simplicities in design and operation. However, they are operated in high temperatures and produce a low-yield desired product. Temperature management is an important factor in the ODHE process since it affects the selectivity of ethylene as a main index for the ethylene production [13,22]. Oxygen consumption procedure plays a vital role in the heat generation and temperature profile inside the reactor. Another important factor is the role of coolant type on the tem-

†To whom correspondence should be addressed.
E-mail: j_karimi@alum.sharif.edu
Copyright by The Korean Institute of Chemical Engineers.

perature profile. Liquid phase coolants are more appropriate than gas phase coolants because of the high heat capacity and good heat transfer coefficient. Although the heat generation rate in membrane reactors is lower than fixed bed reactors due to the gradual permeation of air and cold shots, the air stream cannot remove the reaction heat efficiently [19,23,24].

As mentioned earlier, oxygen has a considerable impact on the temperature profile and selectivity of ethylene; hence, the oxygen distribution along the reactor will improve its performance. Although membrane reactors can distribute axially oxygen injection in the reaction side, their application from an industrial point of view is very limited because of their aforementioned drawbacks. Despite high operating temperature and low-yield products of fixed bed reactors, they are commonly used in industries yet. Therefore, a strategy to improve the performance of the fixed bed reactor for the ODHE process in terms of operational temperature and products yield is worthy of investigation, so that this reactor capacity inclines to the membrane reactor while keeping its industrial application. Side feeding reactor with sectional air injections appears to be a good alternative, in which the inlet oxygen is divided into several sub-streams injected along the body of fixed bed reactor instead of completely feeding at the reactor's entrance. As a result, the oxygen partial pressure could be better controlled in the reaction zone, thereby approaching to the performance of membrane reactor [22,25,26].

We developed a one-dimensional non-isothermal steady state model to study the ODHE process in three different reactor configurations, i.e., side feeding reactor (SFR), conventional fixed bed reactor (CFBR) and membrane reactor (MR). The performance capability of the three type reactors was compared in terms of conversion of ethane and oxygen, selectivity of ethylene and carbon dioxide as well as temperature of the reaction zone. Also, the sensitivity analysis was carried out and the effect of the location and amount of the air injection on the performance of the ODHE process in the SFR was investigated.

KINETIC MODEL

A power law kinetic rate equation has been applied in mathematical modeling for the set of reactions presented by Eqs. (1)-(3):

$$C_2H_6+\frac{1}{2}O_2\rightarrow C_2H_4+H_2O \quad (1)$$

$$C_2H_6+\frac{7}{2}O_2\rightarrow 2CO_2+3H_2O \quad (2)$$

$$C_2H_4+3O_2\rightarrow 2CO_2+2H_2O \quad (3)$$

Heracleous and Lemonidou [27,28] proposed this kinetic model for the ODHE process over a Ni-Nb-O mixed oxides catalyst that has high activity and selectivity. The rate equation is shown in Eq. (4) and the corresponding kinetic parameters have been listed in Table 1.

$$R_j=k_{R,j}\exp\left[-\frac{E_j}{R}\left(\frac{1}{T}-\frac{1}{T_R}\right)\right]p_{HC_j}^{m_j}p_{O_2}^{n_j} \quad (4)$$

Table 1. Kinetic parameters of reactions

Equation no.	E_j (kJ/kmol)	$K_{R,j}$ (kmol/($kg_{cat}p^{m+n}s$))	m_j	n_j
1	96180	4.177×10^{-10}	0.520	0.213
2	76210	1.272×10^{-13}	0.547	0.829
3	98420	9.367×10^{-11}	0.475	0.319

REACTOR MODEL

A one-dimensional steady-state model was developed [29] to model the ODHE process in CFBR, SFR and MR. The general following assumptions were made in developing the mathematical model for the three types of reactors [22,24,25,29]:

1. Radial profiles of concentration and temperature were neglected due to the small diameter of tubes.
2. A steady state and non-isothermal/non-adiabatic operation was considered.
3. External mass diffusion resistance and axial dispersions on both the tube and shell sides were considered to be negligible as a consequence of high flow rate of the streams.
4. Internal mass transfer resistance was ignored because of the small diameter of catalyst particles.
5. Gas follows the ideal gas law to determine the partial pressures from the molar flows.

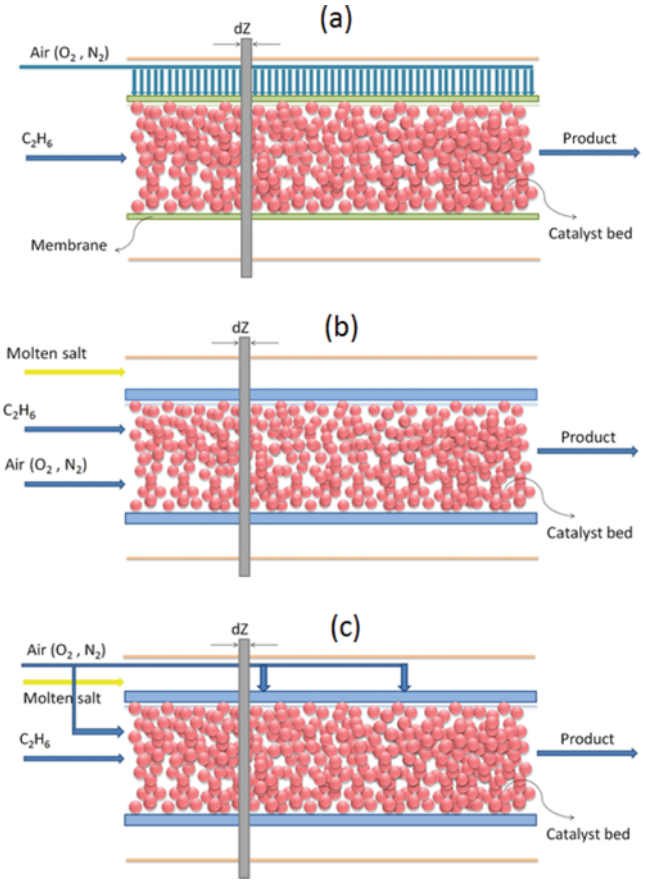

Fig. 1. Schematic diagram of (a) membrane reactor (MR), (b) conventional fixed bed reactor (CFBR) and (c) side feeding reactor (SFR2).

6. No heat loss was considered for the shell side.

7. A co-current design was adopted between the shell and tube side streams leading to a better heat management.

8. In the oxidative dehydrogenation process, any coke deposited on the catalyst would be oxidized by oxygen so that catalyst activity is retained [14]. Therefore, the coke formation in combustion reactions and deactivation of the catalysts and membrane was ignored in the model.

1. Membrane Reactor Model

The membrane reactor configuration is shown in Fig. 1(a). As depicted, only the ethane is fed at the reactor inlet and the air is permeated gradually through the membrane. The air also acts as a coolant in the shell side. The heat and mass transfer resistances of the gas films at the both sides of the membrane wall were assumed to be negligible. The balance equations for the tube side are as follows:

Mass balance:

$$\frac{dF_i^t}{dZ} = n_t \pi r_1^2 \rho_B \sum_{j=1}^{3} \nu_{ij} R_j \quad i = C_2H_6,\ C_2H_4,\ CO_2,\ H_2O \tag{5}$$

$$\frac{dF_i^t}{dZ} = n_t 2\pi r_1 J_i + n_t \pi r_1^2 \rho_B \sum_{j=1}^{3} \nu_{ij} R_j \quad i = O_2,\ N_2 \tag{6}$$

Energy balance:

$$\frac{dT^t}{dZ} = \frac{n_t \pi r_1^2}{\Sigma_{i=1}^{6} F_i^t Cp_i^t}\left[\rho_B \sum_{j=1}^{3}(-\Delta H_{Rj} R_j) - \frac{2}{r_1}(J_{O_2} Cp_{O_2}^t + J_{N_2} Cp_{N_2}^t + U)(T^t - T^s)\right] \tag{7}$$

Momentum balance:

$$\frac{dP^t}{dZ} = -f\frac{\rho_g u^2}{d_p} \tag{8}$$

The balance equations for the shell side are as follows:

Mass balance:

$$\frac{dF_i^s}{dZ} = -n_t 2\pi r_2 J_i \tag{9}$$

Energy balance:

$$\frac{dT^s}{dZ} = \frac{n_t 2\pi r_2}{\sum_{i=1}^{2} F_i^s Cp_i^s}[U(T - T^s)] \quad i = O_2,\ N_2 \tag{10}$$

An inorganic porous membrane was used in the MR that is non-selective to oxygen. This kind of membrane has a higher permeation flux in respect of the dense membranes. The energy balance of tube side (Eq. (7)) contains the heat production by chemical reaction, energy associated with the air permeating flux and the heat exchanged between the shell side and the tube side. The heat produced by reactions and the air permeating flux is not present in the energy balance Eq. (10) on the shell side. The permeation flux of the membrane is described as follows and the geometric parameters of the membrane are listed in Table 2 [18,30].

$$J_i = -\frac{1}{RT_m}\left[\frac{D_i^e}{\delta}(p_i - p_i^s) + \frac{B_0}{\delta \mu_i} p_i^s (P^t - P^s)\right] \quad i = O_2,\ N_2 \tag{11}$$

Table 2. Membrane characteristics

Parameter	Value
K_0 (m)	23.1×10^{-10}
B_0 (m^2)	11.5×10^{-17}
δ (m)	17.5×10^{-4}

$$D_i^e = K_0\sqrt{\frac{8RT_m}{\pi M_i}} \tag{12}$$

2. Conventional Fixed Bed Reactor Model

A schematic diagram of CFBR is shown in Fig. 1(b). As the figure illustrates, in this type of reactor both reactants (ethane and air) are fed into the tube side and the coolant (molten salt) flows through the shell side. A preheating zone was considered for ODHE fixed bed reactors to increase the temperature of inlet feed [22]. In this region that is filled with inexpensive inert particles, the temperature of feed increases from 100 °C to 350 °C. This inlet temperature provides noticeable reaction rates as a consequence of reaction ignition. An approximate temperature drop of 20 °C occurs in the shell side for the coolant. Based on the mentioned assumptions, the balance equations of the CFBR modeling for the tube side are as follows:

Mass balance:

$$\frac{dF_i^t}{dZ} = n_t \pi r_1^2 \rho_B \sum_{j=1}^{3} \nu_{ij} R_j \quad i = C_2H_6,\ C_2H_4,\ CO_2,\ H_2O,\ O_2,\ N_2 \tag{13}$$

Energy balance:

$$\frac{dT^t}{dZ} = \frac{n_t \pi r_1^2}{\Sigma_{i=1}^{6} F_i^t Cp_i^t}\left[\rho_B \sum_{j=1}^{3}(-\Delta H_{Rj} R_j) - \frac{2}{r_1}U(T^t - T^s)\right] \tag{14}$$

and for the shell side:

Energy balance:

$$\frac{dT^s}{dZ} = \frac{n_t 2\pi r_2}{F^s Cp^s}[U(T^t - T^s)] \tag{15}$$

3. Side Feeding Reactor Model

The side feeding reactor (SFR2 (with two injection points)) is illustrated in Fig. 1(c). According to the number of injections, the total air flow is equally divided to several parts. One part is fed at the reactor inlet with the ethane feed and the rest parts are injected into the body of the reactor at the same intervals, as shown in Fig. 1(c). Again, the molten salt is used as a coolant in the shell side and there is an inert region for preheating the feed with the same condition of CFBR. The balance equations of the SFR for each injection section are the same as CFBR.

NUMERICAL SIMULATION

The pressure drop in momentum balance equations was calculated from the Ergun equation. The overall heat transfer (U) in energy balance equations was evaluated based on Froment and Bischoff [31] suggestions and estimated as resistances in series on the reaction and permeation sides. The heat-transfer coefficient for the tube side was calculated by means of Leva's correlation [31]

and that corresponding to the permeation side was calculated using the correlation suggested by Kern [32]. The properties of molten salt were taken from Rose [10]. Three sets of ordinary differential equations (ODEs) obtained from the balance equations for the CFBR, SFR and MR were solved numerically using fourth-order Runge-Kutta method. To solve the set of ODEs, the required initial conditions are defined at the inlet of the three kinds of reactors as follows:

$$F^{t}_{i,\,z=0} = F^{t}_{i,\,in} \tag{17}$$

$$T^{t}_{z=0} = T^{t}_{in} \tag{18}$$

$$P^{t}_{z=0} = P_0 \tag{19}$$

$$F^{s}_{i,\,z=0} = F^{s}_{i,\,in} \tag{20}$$

$$T^{t}_{z=0} = T^{s}_{in} \tag{21}$$

To compare the performance of the three types of reactors, conversion of ethane, selectivity of ethylene and carbon dioxide, and temperature of the reactor were considered as the comparing responses. The same rate of ethylene production was adopted as the basis of comparison. It was achieved by adjusting the shell side pressure in MR. As a first step in the present simulation, one injection point was considered for the SFR. It means that the total air flow was divided into two parts with the same amount of molar flow rate. The first part was introduced with ethane at the reactor inlet and the other one injected at the middle of the reactor (SFR1). As a next step, the influence of increasing the number of injection points on SFR performance was also studied. For example, SFR2 represents the condition that the total air flow was equally divided into three streams. One of these streams feeds into the reactor at the entrance, and the next two streams are injected into the wall of reactor at same intervals (as shown in Fig. 1(c)). The active zone (catalyst particles zone) results of CFBR and SFR are represented in diagrams. The effects of amount and location of the air injection points were also investigated. Bed characteristics and operating conditions of the reactors are shown in Table 3 [19,22,24,29].

Table 3. Bed characteristics and operating conditions

Parameter	CFBR, SFR	MR
Tube length, L (m)	4	4
Inner radius of tube, r_1 (m)	0.0133	0.0133
Outer radius of tube, r_2 (m)	0.01505	0.01505
Number of tubes, n_t	10000	10000
Bed density, ρ_b (kg/m^3)	50	50
Void fraction of packing, ε_b	0.48	0.48
Catalyst equivalent diameter, d_p (m)	0.006	0.006
Tube side inlet pressure, P^t (atm)	5	5
Shell side inlet pressure, P^s (atm)	-	5.2-6
Tube side inlet temperature, T^t_{in} (°C)	100	360
Shell side inlet temperature, T^s_{in} (°C)	370	25
Feed flow rate, F^t_{in} (kmol/h)	3000	3000
Coolant flow rate, F^s_{in} (kg/s)	300	24.1
Mole fraction of O_2	0.1	1
Mole fraction of N_2	0.4	0
Mole fraction of C_2H_6	0.5	0
Coolant	Molten salt	Air (O_2, N_2)

The conversion of ethane was calculated from the difference between the inlet and outlet ethane concentrations and the selectivity of ethylene and carbon dioxide was determined using the following equations:

$$S_{C_2H_4} = \frac{(F_{C_2H_4,\,Z} - F_{C_2H_4,\,0})/\nu_{C_2H_4}}{(F_{C_2H_6,\,0} - F_{C_2H_6,\,Z})/\nu_{C_2H_6}} \tag{22}$$

$$S_{CO_2} = \frac{(F_{CO_2,\,Z} - F_{CO_2,\,0})/\nu_{CO_2}}{(F_{C_2H_6,\,0} - F_{C_2H_6,\,Z})/\nu_{C_2H_6}} \tag{23}$$

RESULTS AND DISCUSSION

1. Model Verification

Verification and validation of simulation results is an important issue for the reliability of process simulation. The experimental data reported by Skoufa et al. [33] were considered for fixed bed model verification. The model validity was examined by comparing the simulation and experimental results. Skoufa et al. [33] investigated the ethane oxidative dehydrogenation reaction over $Ni_{0.85}Nb_{0.15}O_x$ mixed oxide catalyst in a bench scale fixed bed reactor (0.9 cm ID

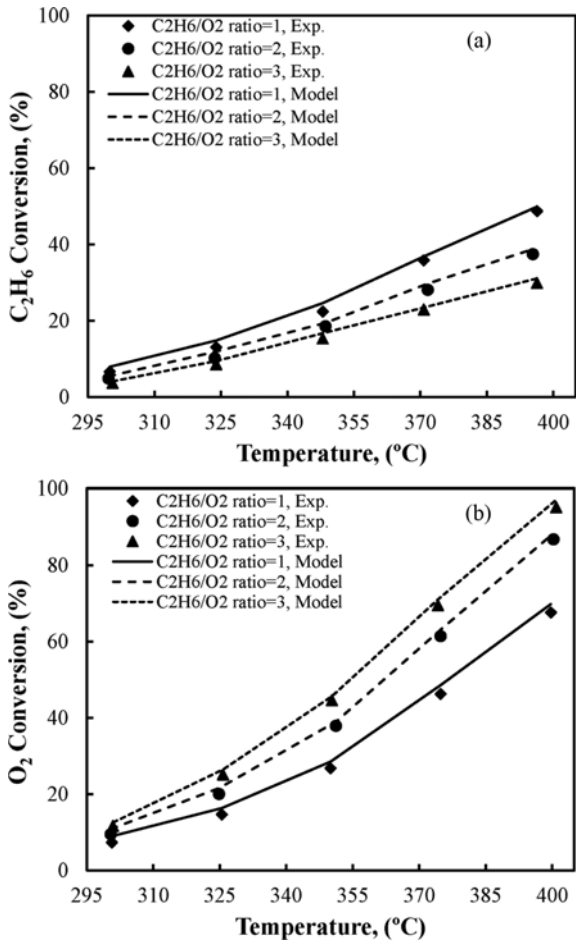

Fig. 2. Comparison of experimental and simulation results for conventional fixed bed reactor: (a) conversion of C_2H_6, (b) conversion of O_2 vs. temperature at different C_2H_6/O_2 ratios.

and 2 cm in length). They studied the ethylene and oxygen conversions as a function of ethane-to-oxygen ratio under steady state conditions between 300 and 400 °C. The operating conditions of the fixed bed rector were considered according to the experimental data of Skoufa et al. [33] The fixed bed model and experiment are compared in Fig. 2. The model predictions are in close agreement with the experimental data.

There is no published experimental data of the ODHE reaction in a membrane reactor. Therefore, the results obtained for membrane reactor were compared with the model results proposed by Rodriguez et al. [19] They presented a theoretical study of a multitubular packed-bed membrane reactor for ODHE reaction over the Ni-Nb-O mixed oxide catalyst. The comparisons of tube-side and shell-side temperatures vs. axial position for different inlet oxygen content at inlet feed temperature of 360 °C are in Fig. 3(a). When no O_2 is fed to the tube mouth (% O_2=0), the temperature profile of tube side decreases monotonically along the reactor. Since the reaction rates are very low, the heat generation rate in the tube side is lower than the heat transfer rate toward the shell side. In the case of 1% O_2, a flat temperature profile is observed in the first 1.5 m of the tube. Beyond this axial position, the reaction ignites and the temperature profile shows a relatively sharp increase. When 5% O_2 is fed to the tube mouth, a sharp temperature rise occurred

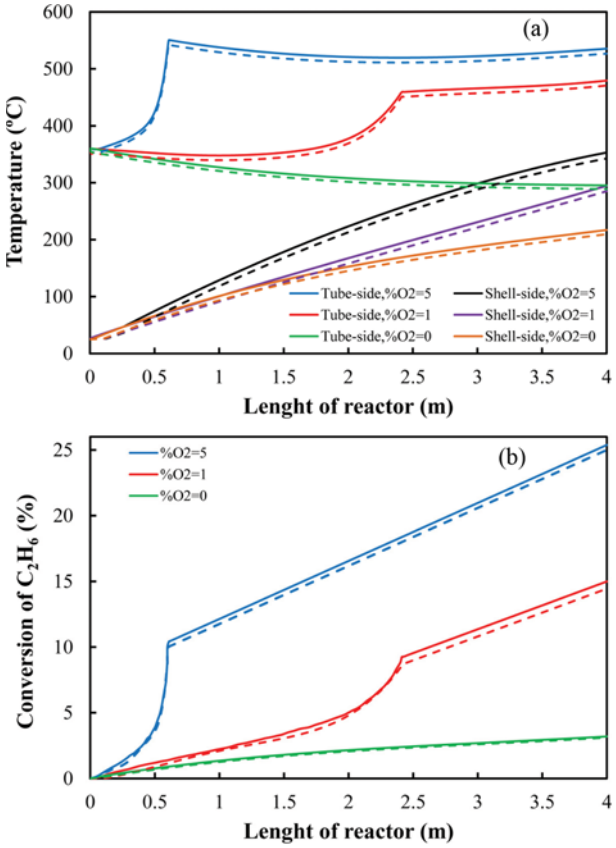

Fig. 3. Comparison of proposed model (dashed lines) and Rodriguez et al. [19] model (solid lines) results for membrane reactor: (a) tube-side and shell-side temperatures, (b) conversion of C_2H_6 vs. axial position at different inlet oxygen contents, T_f=360 °C.

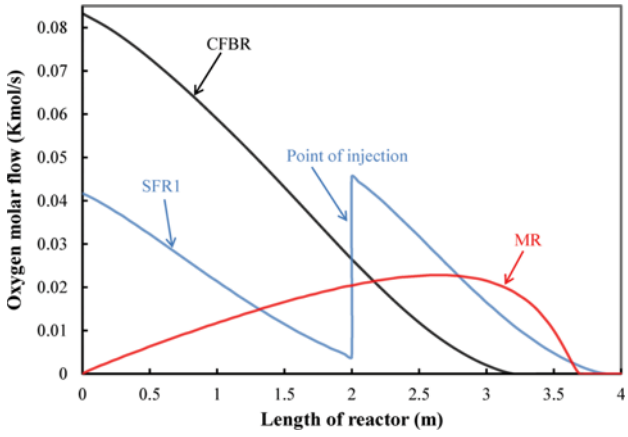

Fig. 4. Oxygen flow rate in tube side of CFBR, SFR1 and MR vs. axial reactor coordinate.

because of fast reactor ignition. Fig. 3(a) also shows that there are close agreements between the results of the two models. Moreover, an analogy between the two models in terms of the axial profiles of ethane conversion at different inlet oxygen contents is shown in Fig. 3(b). As can be seen, ethane conversion increases with the increase of inlet oxygen contents. As previously mentioned, as the oxygen content increases, the reaction can be ignited more rapidly and the ethane conversion tends to improve. Fig 3(b) also demonstrates that the model presented in this study is in accordance with the model of Rodriguez et al. [19].

2. Comparison of the Three Reactors

As mentioned, the oxygen partial pressure in the reaction side has an extremely significant influence on the ODHE performance, particularly in the cases of temperature and selectivity of ethylene axial profiles. Fig. 4 shows the oxygen molar flow along the length of three types of reactors (CFBR, MR and SFR1). CFBR has higher O_2 partial pressure. Although the oxygen content in the MR is lower than two other reactors, an unfavorable accumulation of O_2 is observed in the tube side of the MR. O_2 accumulation not only lowers the ethylene selectivity, but also could be the origin of hot spots and explosion in some operating conditions. In the first 3 meters of the reactor, the reaction rate is not high enough and the rate of O_2 permeation through the membrane is higher than the rate of O_2 consumption. Thus, the O_2 molar flow increases in this region and thereafter (Z=3) with increasing the amount of O_2 and reactor temperature the reaction ignites and oxygen depletion occurs. The O_2 molar flow trend of the SFR1 shows the best pattern of oxygen consumption due to the low amounts of oxygen without any accumulation. The gradual increase in the partial pressure of oxygen in the membrane reactor (as seen in the Fig. 4) is undesired, since it can lead to safety problems such as the occurrence of explosive mixtures. By increasing the injection number, the O_2 partial pressure will further decrease and lie under the MR graph.

The conversion of ethane as a function of the reactor length is shown in Fig. 5. The value of ethane conversion for the MR is very low in comparison with the CFBR and SFR1 conversions, resulting from the limitation of air permeation through the membrane. Regarding the MR, the axial conversion profile has a smooth slope at the beginning due to the low rate of reaction; however, a rela-

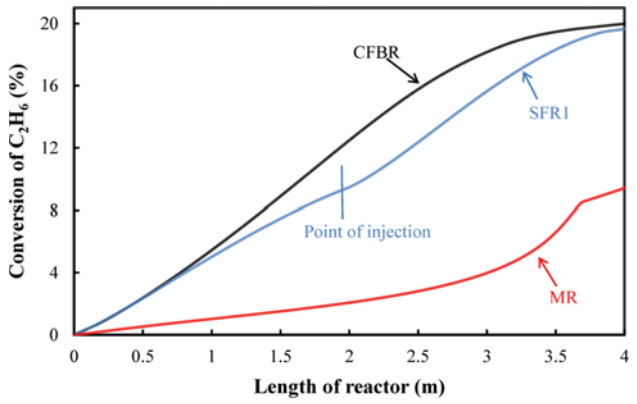

Fig. 5. Conversion of C_2H_6 in CFBR, SFR1 and MR vs. axial reactor coordinate.

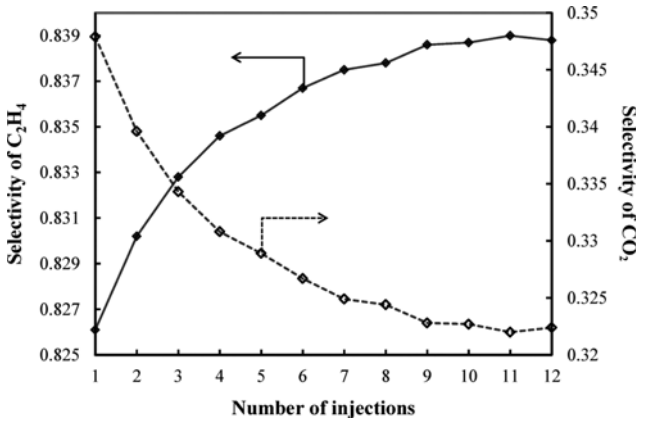

Fig. 7. Selectivity of C_2H_4 and CO_2 in SFR vs. number of injections.

tively sharp increase is observed after Z=3 m because of the reaction ignition, as shown in Fig. 4. The conversion of ethane for the SFR1 is lower than the CFBR along the length of reactor, but the air fresh injection at the middle of reactor increases the conversion, as the outlet conversion is almost 19.7%, a comparable value with the CFBR conversion.

The ethylene selectivity is the main index of ODHE performance and the overall plant yield [22]. Controlled oxygen consumption can largely improve the selectivity of ethylene in the ODHE process. As previously mentioned, CO_2 is an undesirable product of the total oxidation reactions (Eqs. (2) and (3)). The comparison of reaction orders with respect to oxygen for the reactions (1)-(3) indicates that high oxygen partial pressure in the reaction side can cause undesired reactions and increase the CO_2 production. Furthermore, these exothermic reactions will influence the temperature profile and rise the rector temperature. The selectivity of ethylene and CO_2 for the three types of reactors are shown in Fig. 6. MR has the highest ethylene selectivity level and the lowest one for CO_2 due to the controlled permeation of oxygen. Although the ethylene selectivity profile increases with a smooth slope up to Z=3 m because of the O_2 accumulation, after that the increase in the reaction rate enhances the ethylene production and achieves the highest value for the selectivity of ethylene. Introducing the

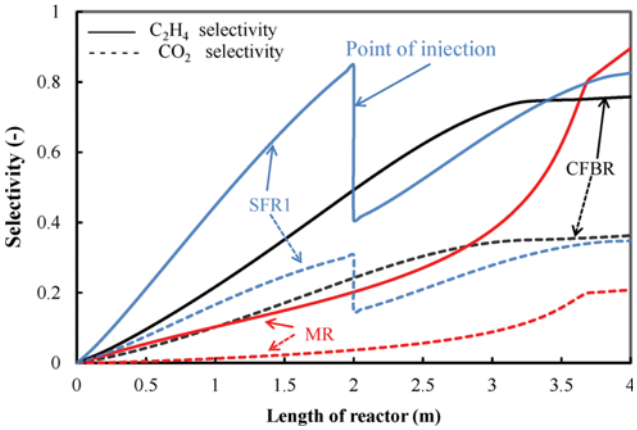

Fig. 6. Selectivity of C_2H_4 and CO_2 in CFBR, SFR1 and MR vs. axial reactor coordinate.

whole oxygen with ethane at the entrance of CFBR leads to a low selectivity of ethylene. Compared to the CFBR, in the SFR1 the ethylene selectivity profile has a sharp slope along the reactor due to the low partial pressure of oxygen and the higher value at the reactor outlet.

A selectivity drop is observed at the point of injection for the SFR1 caused by the high amount of oxygen at this point. By increasing the number of injections, the selectivity of ethylene and CO_2 will improve and approach to the MR performance, as depicted in Fig. 7. With the increase of injection points, the C_2H_4 selectivity increases from 0.826 to 0.839 and that of CO_2 decreases from 0.348 to 0.322. This figure also shows that the performance of ODHE process is improved up to nine injections; however, further injections (SFR>9) have a little bit of an effect on the selectivity of ethylene and CO_2.

Reactor temperature control is a key factor in the ODHE process. The reduction of reactor temperature under 350 °C decreases the rate of reaction (1); however, temperature over-increase will aggravate the ethylene production and induce the formation of hot spots. The axial temperature profiles of reactors are shown in Fig. 8(a). The MR has a different and undesirable temperature profile in comparison with the CFBR and SFR1. Although the generation of heat in the membrane reactors is lower than conventional reactors due to the policy of oxygen distribution, the gas-cooled medium of MR is not able to remove effectively the heat of reactor. The CFBR and SFR1 have an efficient heat removal as a result of molten salt cooling medium.

Regarding the MR, first (Z<1.2) the reactor temperature is decreasing because of the low heat generation and cold inlet air in the shell side (25 °C). By increasing the reaction rate and heat generation, the temperature profile shows an inverse behavior and proceeds with a sharp slope and consequently obtains a high reactor outlet temperature (466 °C). The low reactor outlet temperature and milder profiles for the CFBR and SFR show a better heat management. A relatively sharp increase is observed for the CFBR at the reactor inlet due to the high amount of oxygen introduced with the ethane at the reactor entrance. This figure also illustrates that the side feeding procedure leads to a relatively smooth profile and a lower hot spot compared to the CFBR. A temperature drop occurs in the injection point because of the fresh air injection as a

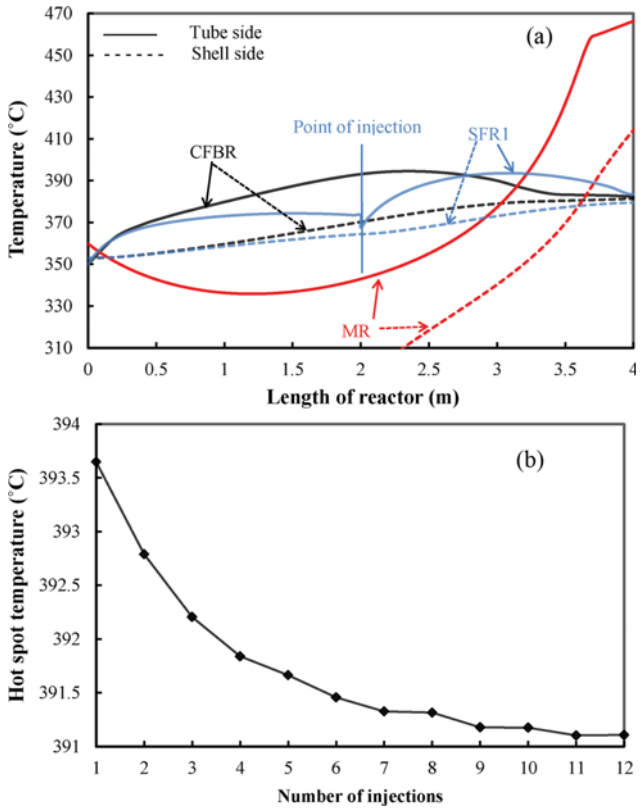

Fig. 8. (a) Temperature profile of tube and shell side in CFBR, SFR1 and MR vs. axial reactor coordinate, (b) Hot spot temperature in SFR vs. number of injections.

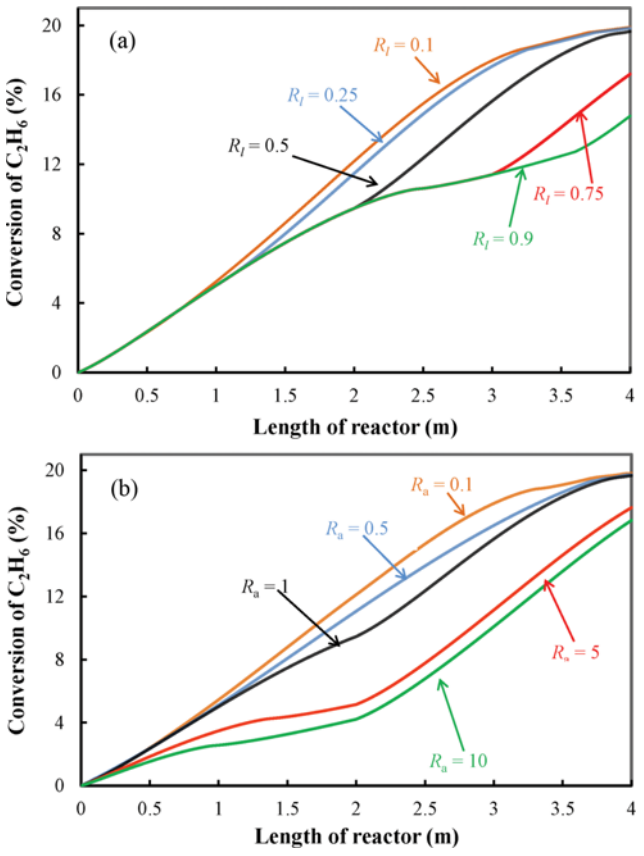

Fig. 9. Conversion of C_2H_6 in SFR1 vs. axial reactor coordinate at different values of (a) R_l and (b) R_a.

cold shot. By increasing the injection points, the maximum temperature of SFR profile will further decrease, as shown in Fig. 8(b).

To investigate the influence of the location and amount of air injections on the ODHE performance in the SFR, two parameters are defined as follows:

$$R_l = \frac{L_z}{L} \tag{24}$$

$$R_a = \frac{F^b_{air}}{F^i_{air}} \tag{25}$$

in which, L_z denotes the distance of injection point from the reactor inlet and L shows the length of reactor. F^b_{air} is the amount of air injected in the body of reactor and F^i_{air} represents the amount of air fed at the inlet of reactor. The influence of different values of R_l and R_a was studied on the selectivity and conversion of ethane and temperature profiles in the SFR and discussed below.

Figs. 9(a) and (b) show the influence of R_l and R_a on the ethane conversion along the reactor length. As R_l and R_a decrease, the conversion of ethane increases and approaches to the CFBR performance as discussed earlier. Likewise, the selectivity of ethylene and CO_2 as function of R_l and R_a is depicted in Figs. 10(a) and (b). The results of these figures show that the increase of the parameters R_l and R_a improve the selectivity of C_2H_4, whereas the CO_2 selectivity continues to decline with growing these parameters. As shown in Fig. 10(a), with the increase of R_b the C_2H_4 selectivity

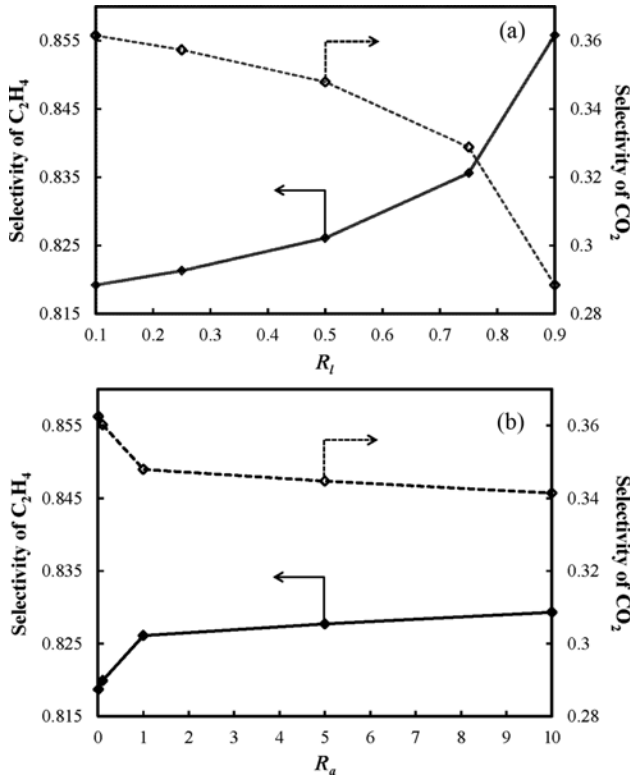

Fig. 10. Selectivity of C_2H_4 and CO_2 in SFR1 vs. (a) R_l and (b) R_a.

increases from 0.819 to 0.856 and that of CO_2 decreases from 0.362 to 0.288. In the case of R_a (Fig. 10(b)), C_2H_4 selectivity increases from 0.818 to 0.829 and that of CO_2 decreases from 0.363 to 0.342. Moreover, the ethylene and CO_2 selectivity profiles for different values of R_b as an example, through the reactor length are shown in Fig. 11. For R_l=0.25, in spite of a sudden increase in the selectivity at the reactor inlet, a sharp drop in the injection point results in a lower amount of outlet selectivity. However, for R_l=0.75, the selectivity drop is smaller at the injection point. Since the location of injection point approaches the reactor outlet, the oxygen content in the injection point decreases leading to a smaller drop in this point.

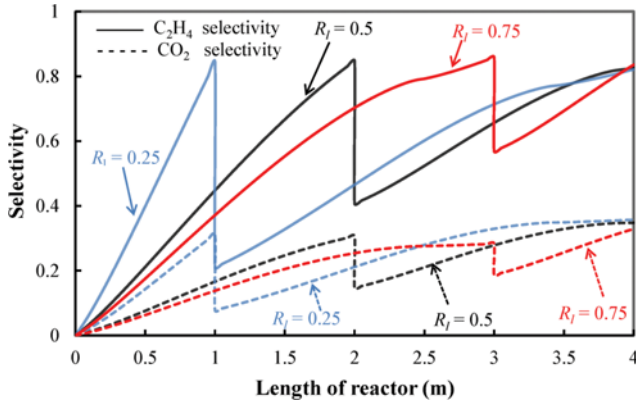

Fig. 11. Selectivity of C_2H_4 and CO_2 in SFR1 vs. axial reactor coordinate at different values of R_l.

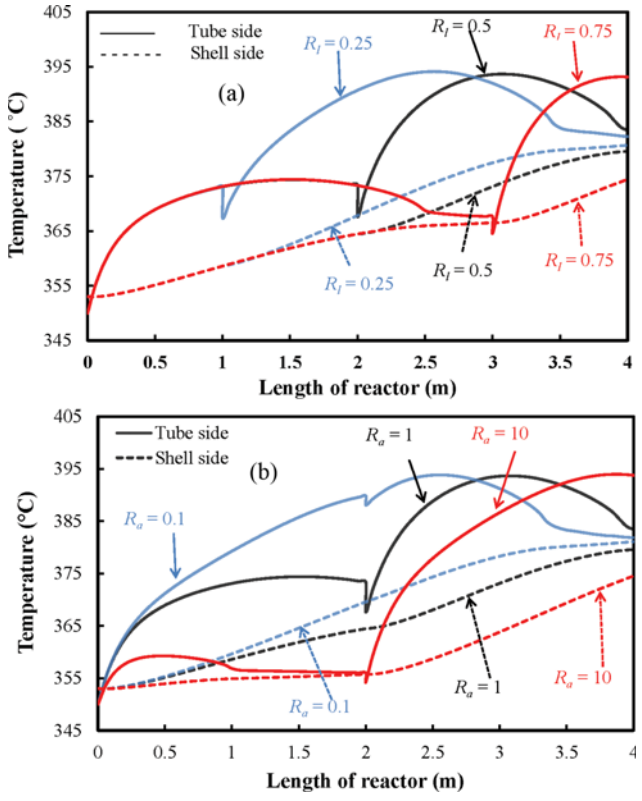

Fig. 12. Temperature profile of tube and shell side in SFR1 vs. axial reactor coordinate at different values of (a) R_l and (b) R_a.

In addition, the temperature profiles reveal that in (Fig. 12(a)) and (Fig. 12b), the reactor temperature is decreasing for Z>2.5. It is a consequence of reaction rate reduction. However, in R_l=0.75 (Fig. 12(a)) and R_a=10 (Fig. 12(b)), the air injection at this point reignites the reaction at the reactor outlet. Increasing temperature leads to an increment in reaction rate, which causes an appreciable value of ethylene selectivity. Moreover, as illustrated in Figs. 12(a) and (b), the maximum temperature of reactor is slightly lower for R_l=0.75 and R_a=10. Future studies should be carried out to find out optimum values of the parameters R_l and R_a for SFR>1 leading to the maximize yield of the ethylene.

CONCLUSION

The performance of three reactor configurations, conventional fixed bed reactor (CFBR), membrane reactor (MR), and side feeding reactor (SFR), in the oxidative dehydrogenation of ethane (ODHE) to ethylene was comprehensively compared. It was found that:

(1) The conversion of ethane for the membrane reactor is very low in comparison with the CFBR and one-side feeding reactor (SFR1) due to the limitation of air permeation through the membrane.

(2) Among these reactor configurations, MR has the highest ethylene selectivity level and the lowest one for CO_2 due to the controlled permeation of oxygen.

(3) As shown in the figures, the performance of one-side feeding reactor was determined between MR and CFBR. By increasing the number of injections in the SFR, the selectivity of ethylene and CO_2 will improve and its performance approaches to the results of MR. Also, increasing the number of injections beyond nine injections has a subtle effect on the performance of SFR.

(4) The temperature profile of MR is different and undesirable in comparison with CFBR and SFR1 since the gas-cooled medium of MR is not able to remove the heat of reactor effectively. The CFBR and SFR1 have a high heat removal as a result of molten salt cooling medium.

(5) The location and amount of air injections highly influence on the performance of SFR. Indeed, the conversion and selectivity of ethylene in the SFR1 increase when the air injection point approaches to the end of reactor. The ethylene conversion of SFR1 decreases with increase of the molar flow rate of side feed, but it has a bit of influence on the ethylene selectivity.

In conclusion, the side feeding reactor with molten salt as a coolant medium could increase selectivity and ethylene production because of the lower oxygen partial pressure along the reactor. Meanwhile, low partial pressure of oxygen without any accumulation in tube side makes a safe reactor for ODHE to ethylene process. This reactor presents an appreciable level of selectivity and avoids the high cost of membrane reactors. The air injection along the reactor prepares an efficient means to improve the ethane conversion and ethylene selectivity as well as temperature control.

NOMENCLATURE

B_0 : geometric parameter of the membrane [m^2]
C_p : heat capacity [kJ $mol^{-1}K^{-1}$]

d_p : catalyst equivalent diameter [m]
D^e : effective Knudsen diffusion coefficient [$m^2\ s^{-1}$]
E : activation energy of reaction [kJ $kmol^{-1}$]
f : friction factor
F : molar flow rate [kmol s^{-1}]
J : permeation flux [kmol $m^{-2}\ s^{-1}$]
K_0 : geometric parameter of the membrane [m]
K_R : rate constant of reaction [kmol $kg_{cat}^{-1}\ p^{-m-n}\ s^{-1}$]
L : length of reactor [m]
M : molecular weight [kg $kmol^{-1}$]
n_t : number of tubes
p : partial pressure [Pa]
P : total pressure [Pa]
r_1 : inner radius of tube [m]
r_2 : outer radius of tube [m]
R : ideal gas constant [kJ $kmol^{-1}\ K^{-1}$]
R_j : instinct rate of j^{th} reaction [kmol $kg_{cat}^{-1}\ s^{-1}$]
S : selectivity
T : temperature [K]
T_m : average temperature of tube side and shell side [K]
T_R : reference temperature and equals 543 K
U : overall heat transfer coefficient [kJ $S^{-1}\ m^{-2}\ K^{-1}$]
u : superficial gas velocity [m s^{-1}]
Z : axial coordinate [m]

Greek Letters

ε_b : void fraction of packing [$m^3 m^{-3}$]
δ : membrane thickness [m]
ν : stoichiometric coefficient
ρ_b : bulk density of catalyst [kgm^{-3}]
ρ_g : gas density [kgm^{-3}]
ΔH : heat of reaction [kJ $kmol^{-1}$]
μ : viscosity [Pa s]

Subscripts

i : component i
j : reaction j
l : related to injection section l in SFR
in : rector inlet
C_2H_6 : ethane
C_2H_4 : ethylene
CO_2 : carbon dioxide
N_2 : nitrogen
O_2 : oxygen
0 : at the axial coordinate z=0

Superscripts

s : shell side
t : tube side

REFERENCES

1. W. Weng, M. Davies, G. Whiting, B. Solsona, C. J. Kiely, A. F. Carley and S. H. Taylor, *PCCP*, **13**, 17395 (2011).
2. I. Popescu, Z. Skoufa, E. Heracleous, A. Lemonidou and I.-C. Marcu, *PCCP*, **17**, 8138 (2015).
3. G. Tsilomelekis and S. Boghosian, *PCCP*, **14**, 2216 (2012).
4. Z. Lin, S. Zhong and D. Grierson, *J. Exp. Bot.*, **60**, 3311 (2009).
5. M. McCoy, M. Reisch, A. Tullo, P. Short, J. Tremblay and W. Storck, *Chem. Eng. News*, **84**, 59 (2006).
6. F. Rahmani and M. Haghighi, *Korean J. Chem. Eng.*, **33**, 2555 (2016).
7. D. Ahchieva, M. Peglow, S. Heinrich, L. Mörl, T. Wolff and F. Klose, *Appl. Catal. A: Gen.*, **296**, 176 (2005).
8. F. Cavani, N. Ballarini and A. Cericola, *Catal. Today*, **127**, 113 (2007).
9. J.-I. Yang, J.-N. Kim, S.-H. Cho and K. R. Krishnamurthy, *Korean J. Chem. Eng.*, **21**, 381 (2004).
10. L. M. Rose, *Chemical reactor design in practice*, Elsevier Scientific Pub. Co. (1981).
11. S. J. Kong, J. H. Jun and K. J. Yoon, *Korean J. Chem. Eng.*, **21**, 793 (2004).
12. W. S. Moon, S. B. Park and S.-M. Yang, *Korean J. Chem. Eng.*, **15**, 136 (1998).
13. P. Arpentinier, F. Cavani and F. Trifirò, The Technology of Catalytic Oxidations, Technip, Paris (2001).
14. F. Al-Sherehy, A. Adris, M. Soliman and R. Hughes, *Chem. Eng. Sci.*, **53**, 3965 (1998).
15. J. Armor, *Appl. Catal.*, **49**, 1 (1989).
16. J. Zaman and A. Chakma, *J. Membr. Sci.*, **92**, 1 (1994).
17. H. Wang, Y. Cong and W. Yang, *Catal. Today*, **82**, 157 (2003).
18. M. Pedernera, R. Mallada, M. Meneéndez and J. Santamaria, *AIChE J.*, **46**, 2489 (2000).
19. M. a. L. Rodriguez, D. E. Ardissone, A. A. Lemonidou, E. Heracleous, E. López, M. N. Pedernera and D. O. Borio, *Ind. Eng. Chem. Res.*, **48**, 1090 (2008).
20. C. Y. Tsai, A. G. Dixon, W. R. Moser and Y. H. Ma, *AIChE J.*, **43**, 2741 (1997).
21. C. Tellez, M. Menendez and J. Santamaria, *AIChE J.*, **43**, 777 (1997).
22. E. López, E. Heracleous, A. A. Lemonidou and D. O. Borio, *Chem. Eng. J.*, **145**, 308 (2008).
23. Y. Kao, L. Lei and Y. Lin, *Ind. Eng. Chem. Res.*, **36**, 3583 (1997).
24. M. L. Rodriguez, D. E. Ardissone, E. Heracleous, A. A. Lemonidou, E. López, M. N. Pedernera and D. O. Borio, *Catal. Today*, **157**, 303 (2010).
25. A. M. Dashliborun, S. Fatemi and A. T. Najafabadi, *Int. J. Hydrogen Energy*, **38**, 1901 (2013).
26. W. Kiatkittipong, T. Tagawa, S. Goto, S. Assabumrungrat, K. Silpasup and P. Praserthdam, *Chem. Eng. J.*, **115**, 63 (2005).
27. E. Heracleous and A. Lemonidou, *J. Catal.*, **237**, 175 (2006).
28. E. Heracleous and A. Lemonidou, *J. Catal.*, **237**, 162 (2006).
29. M. a. L. Rodríguez, D. E. Ardissone, E. López, M. N. Pedernera and D. O. Borio, *Ind. Eng. Chem. Res.*, **50**, 2690 (2011).
30. M. Munro, *J. Am. Ceram. Soc.*, **80**, 1919 (1997).
31. G. F. Froment, K. B. Bischoff and J. De Wilde, *Chemical reactor analysis and design*, Wiley New York (1990).
32. D. Q. Kern, *Process heat transfer*, Tata McGraw-Hill Education (1950).
33. Z. Skoufa, E. Heracleous and A. Lemonidou, *Chem. Eng. Sci.*, **84**, 48 (2012).